

# We are IntechOpen, the world's leading publisher of Open Access books Built by scientists, for scientists

**4,100**

Open access books available

**116,000**

International authors and editors

**120M**

Downloads

**154**

Countries delivered to

**TOP 1%**

most cited scientists

**12.2%**

Contributors from top 500 universities



**WEB OF SCIENCE™**

Selection of our books indexed in the Book Citation Index  
in Web of Science™ Core Collection (BKCI)

Interested in publishing with us?  
Contact [book.department@intechopen.com](mailto:book.department@intechopen.com)

Numbers displayed above are based on latest data collected.

For more information visit [www.intechopen.com](http://www.intechopen.com)



# Dynamical Particle Motions in Vortex Flows

---

Steven Wang and Naoto Ohmura

Additional information is available at the end of the chapter

<http://dx.doi.org/10.5772/66315>

---

### Abstract

Circular vortex flows generate interesting self-organizing phenomena of particle motions, that is, particle clustering and classification phenomena. These phenomena result from interaction between vortex dynamics and relaxation of particle velocity due to drag. This chapter introduces particle clustering in stirred vessels and particle classification in Taylor vortex flow based on our previous research works. The first part of this chapter demonstrates and explains a third category of solid-liquid separation physics whereby particles spontaneously localize or cluster into small regions of fluids by taking the clustering phenomena in stirred vessels as an example. The second part of this chapter discusses particle classification phenomena due to shear-induced migration. Finally, this chapter discusses about process intensification utilizing these self-organizing phenomena of particle motions in vortex flows.

**Keywords:** solid-liquid flow, particle classification, particle clustering, chaotic-mixing field, process intensification

---

## 1. Introduction

Vortex motions play an important role for the enhancement of transport phenomena in chemical processes. Utilizing appropriate vortex motions can significantly enhance the energy efficiency of unit operations and make chemical processes more compact and safer. Some process intensification methods are, therefore, closely related to vortex dynamics. A continuous oscillatory-baffled reactor (OBR) proposed by Mackely and Ni [1], which first appeared in 1991, is one of successful novel tubular reactors that offers the prospect of a compact plug-flow reactor with uniform, controllable mixing. The continuous OBR comprises tubes fitted with equally spaced, low-constriction orifice plate baffles having an oscillatory motion superimposed upon the net flow of the process fluid [2]. The combination of the baffles and the oscillatory motion creates vortical flow patterns conductive to efficient heat and mass transfer,

---

whilst maintaining plug flow. On the upstroke of the piston, toroidal vortices are formed above the baffle. The vortices dissipate on the following downstroke of the piston, as similar vortices are formed below the baffle. This constant creation and destruction of vortices results in intensifying local mixing. On the other hand, the baffles are obstacles to axial dispersion, which give a plug-flow residence time distribution. Harvey and Stonestreet [3] conducted a case study of an OBR for a batch saponification process. According to their estimation, the OBR can drastically reduce reactor volume from 75 m<sup>3</sup> of the current batch reactor to 0.5 m<sup>3</sup>, and reaction time required can be reduced from 2 h to 12 min by intensifying local mixing.

A Taylor-Couette flow reactor (TCFR) is another typical example of plug-flow-type reactors. Appearance of pairs of counter-rotating Toroidal vortices called Taylor vortices due to hydrodynamic instability provides a minimal axial dispersion combined with a local mixing intensity in a TCFR. In this sense, a TCFR has the potential for an ideal plug-flow reactor with low shear stress [4], which is suitable for processes dealing with shear-sensitive materials such as crystallizations [5], emulsion polymerization [6], bioprocesses [7] and so on.

Circular vortex flows generate another interesting self-organizing phenomena of particle motions, that is, particle clustering and classification phenomena. These phenomena result from interaction between vortex dynamics and relaxation of particle velocity due to drag. As mentioned above, it has been considered that vortex motions contribute to intensification of mixing. When we do away with this fixed idea, however, we might have a chance to develop a novel process intensification method. This chapter introduces particle clustering in stirred vessels and particle classification in Taylor vortex flow based on our previous research works.

The first part of this chapter demonstrates and explains a third category of solid-liquid separation physics whereby particles spontaneously localize or cluster into small regions of fluids by taking the clustering phenomena in stirred vessels as an example. In the second part of this chapter, particle classification phenomena due to shear-induced migration are discussed. Finally, this chapter discussed about process intensification utilizing these self-organizing phenomena of particle motions in vortex flows in ‘Conclusions’ section.

## 2. Particle trapping in stirred flow

In this section, we aim to propose an unexpected category of solid-liquid separation physics where weakly buoyant particles can migrate into two specific regions of non-turbulent fluid in a mixing vessel. We apply a novel three-dimensional (3D) particle visualization method to expose the real-time trajectories of inertial particles, and the results suggest that particles could deviate from underlying flows, and subsequently form dense clusters. The new finding provides a sound basis for solid-liquid separation technologies.

### 2.1. Experimental set-up and measurements

**Figure 1** shows the schematic of the stirred system, consisting of the overhead motor (Heidolph RZ2102), a Rushton turbine and a cylindrical Perspex vessel. A digital camera (Canon Legria HFR28) was used to take sequential images. In the flow visualization experiments, two 1000W

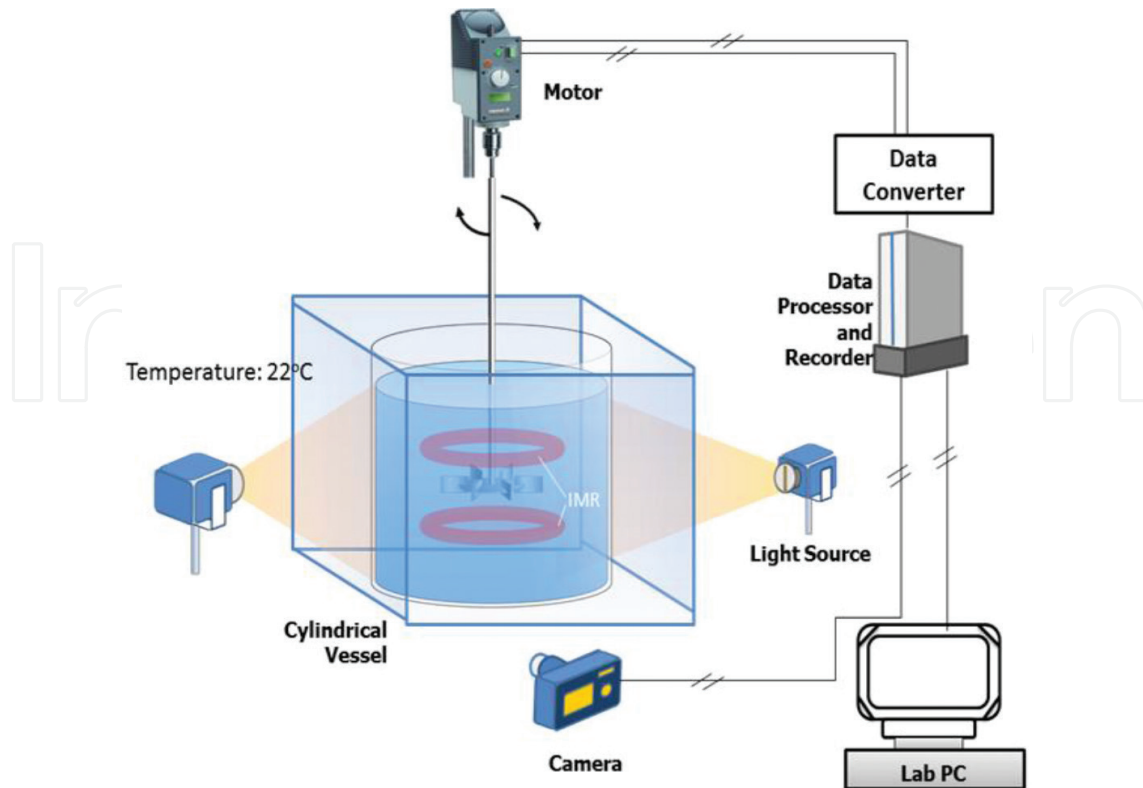


**Figure 1.** Experimental set-up used in this study [8].

Arri IP23 lamps were used [8]. The Rushton impeller is 7 cm in diameter and placed centrally in the vessel along a single shaft. The details of all other impellers are shown in **Figure 2**.

All experiments are completed at modest values of the Reynolds number  $Re$  (here  $Re = \rho N D^2 / \mu < 200$  where  $\rho$  is the fluid density,  $N$  is the rotating speed or in other words the rotating frequency having the dimension of [1/s],  $D$  is the impeller diameter and  $\mu$  is the kinematic viscosity of the fluid).

We use a wide range of particles for the trapping experiments, and  $0.35 \leq \rho_p / \rho_f \leq 1.19$ , and  $0.65 \leq a \leq 7\text{mm}$ , where  $\rho_p$  is the particle density,  $\rho_f$  is the fluid density and  $a$  is the particle diameter. Particles used in the study include polystyrene, ion-exchange resin, polymethyl methacrylate (PMMA), urea resin, rubber particles and wooden particles. Glycerin is used as the working fluids, and is provided by APS Healthcare (Nat Oleo, 99.7% grade). A Bohlin CVO 50-controlled stress rheometer is used to measure the viscosity of the working liquid.

## 2.2. Passive particle motion

Multiphase phase mixing is an important process that takes place throughout the chemical, mineral, food and water industries. Homogenization is the ultimate goal of the mixing devices. In particular, mechanical agitation tanks have been the first mixing-device option for a number of processes essentially due to its versatility, comparative simplicity and effectiveness in providing fast mixing. While multiphase mixing is of highly industrial interests, we

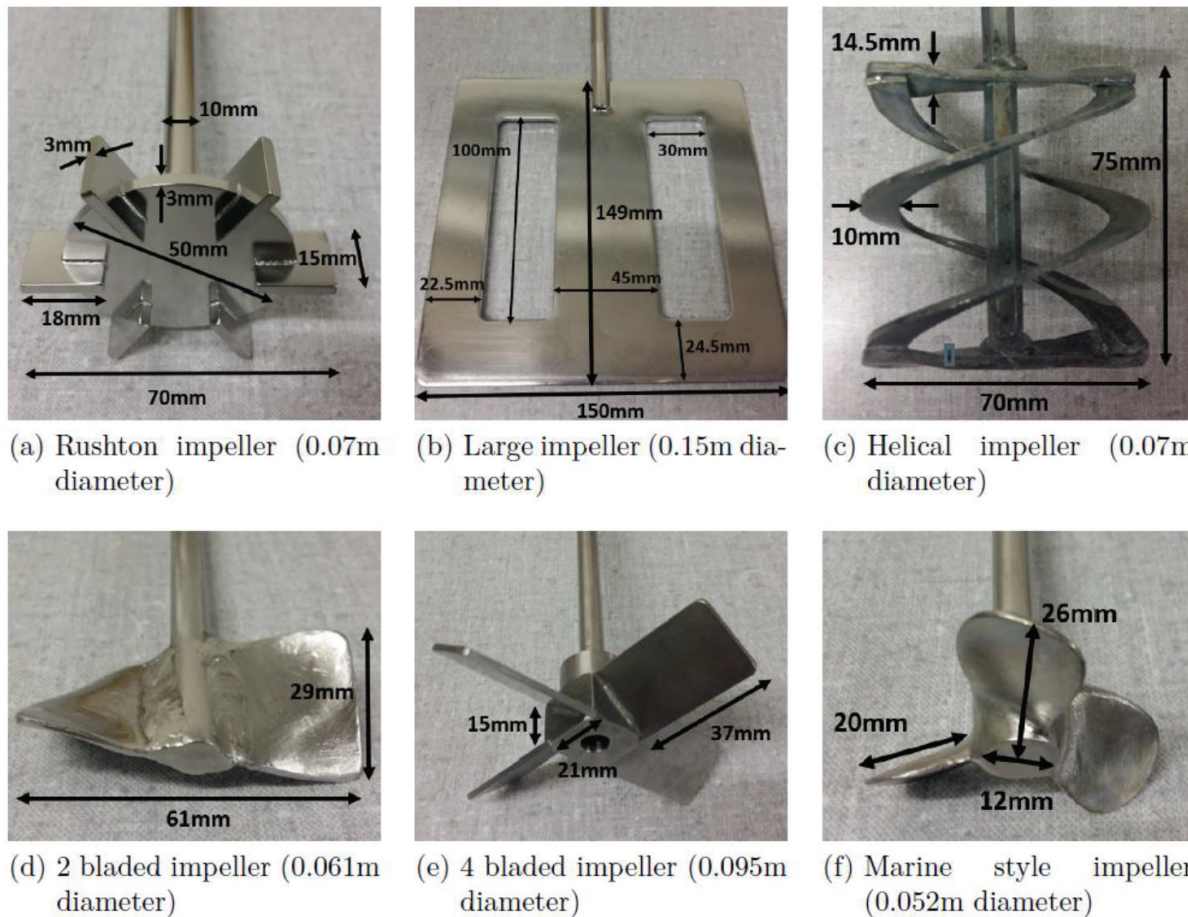


**Figure 2.** Impeller photographs and their dimensions. (a) Rushton impeller; (b) Large impeller; (c) Helical impeller; (d) Two bladed impeller; (e) Four bladed impeller; (f) Marine style impeller.

realize that the prior scientific contributions deal almost exclusively with single-phase fluid-fluid mixing. In this section, we disclose the typical flow mechanism of a ‘standard’ stirred tank that is operated in a low  $Re$  regime.

Laminar stirred tank can produce the complex path lines via chaotic advection. The passing of blades causes the onset of chaos sea by bringing in small perturbations while producing two isolated mixing regions, which are called ‘Kolmogorov-Arnold-Moser (KAM)’ tubes in dynamical system. KAM tubes are the regions of confined mixed zones, segregated by well-defined boundary layer. At low Reynolds numbers, these KAM tubes are present in the form of toroidal vortices. From **Figure 3a**, we can clearly see the chaos sea (stretching and folding areas) as well as the vortex tube, by means of dye-visualization experiment. It is also clearly seen from this picture that the vortex structure is highly complex, consisting of island and filaments. It should be noted that there is no material/fluid exchange between the KAM tubs and the surrounding areas.

In **Figure 3a**, we can consider the dye particles as passive particles. In laminar flows, the Lagrangian motion of a passive particle at location  $\mathbf{X}_p = (X, Y, Z)$  moving according to fluid velocity field  $\mathbf{u} = (u, v, w)$  is mathematically captured by the following kinematic equations:

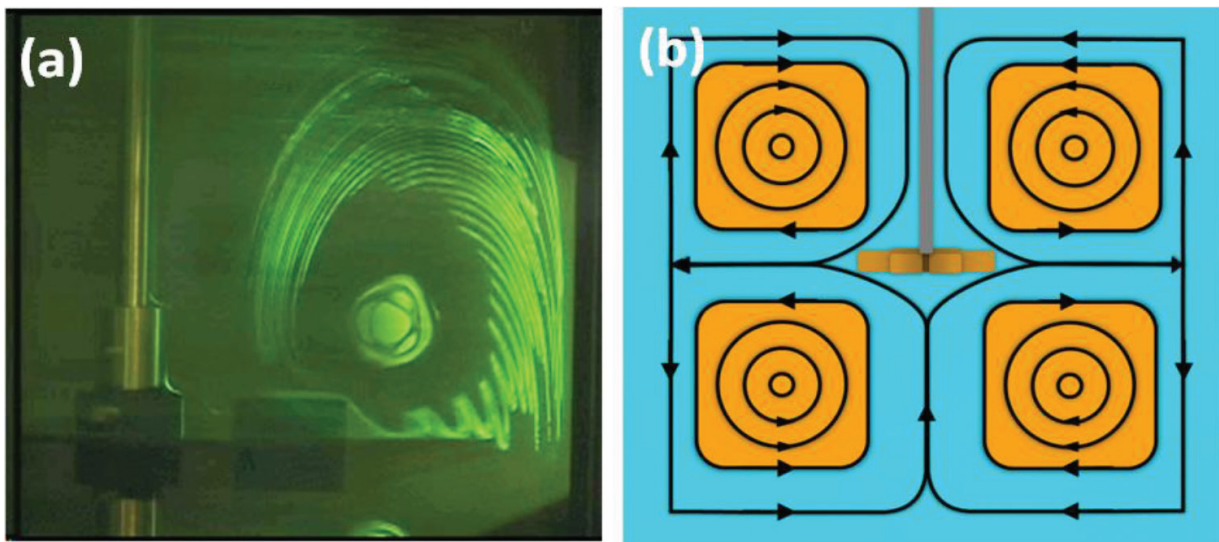


**Figure 3.** (a) Chaotic sea and a KAM tube in the laminar flow system. (b) Fluid particle system for (laminar) stirred tank at low  $Re$ ; two tori present above and below the impeller. Yellow area: KAM tubes (low strain area); the rest of the system: chaotic flow area (high strain area) [8].

$$\begin{aligned} \frac{dX}{dt} &= u(\mathbf{X}_p, t), \\ \frac{dY}{dt} &= v(\mathbf{X}_p, t), \\ \frac{dZ}{dt} &= w(\mathbf{X}_p, t). \end{aligned} \quad (1)$$

The basic assumption in obtaining Eq. (1) is that the small particles do not deviate from the fluid velocities and do not alter the fluid velocities. For passive particles in this low-Reynolds-number flow condition, they always stick to the streamlines in the chaos sea, and do not move into the KAM tubes. The dye-visualization experiment can confirm that, when particles are tiny and spherical, particles move passively along with the respective streamlines. **Figure 3b** shows the conclusive fluid particle system that consists of two tori and surrounding chaotic flow regions.

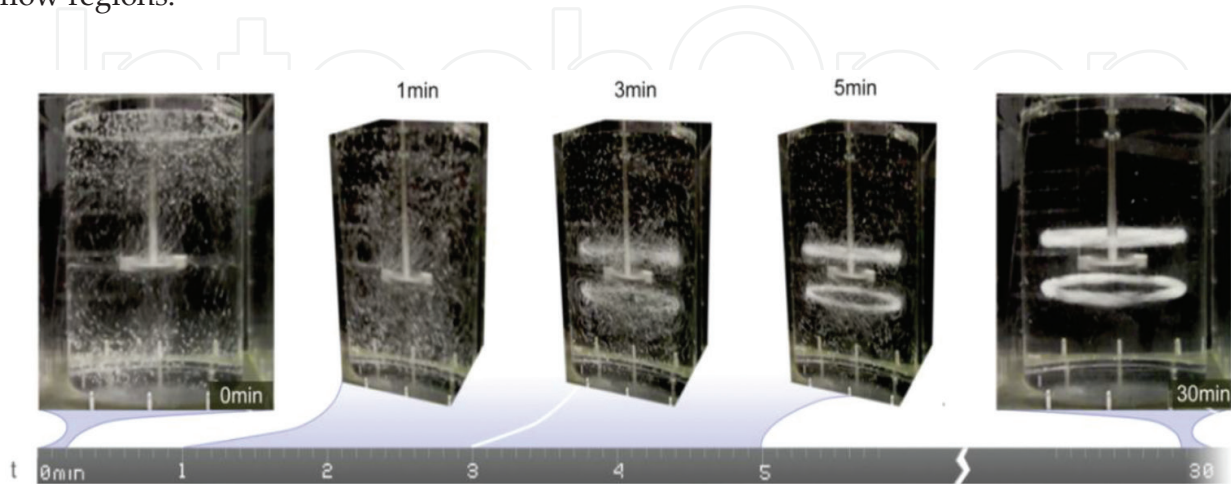


**Figure 4.** Particle trapping in a stirred vessel.  $\rho_p/\rho_f = 0.80$ ,  $a = 1.4$  mm [8].

### 2.3. Inertial particle clustering and criteria

Inertial particles behave completely different from passive ones. As illustrated in **Figure 4**, spherical particles (with  $\rho_p/\rho_f = 0.80$ ,  $a = 1.4$  mm) can deviate their respective streams, and move into the nearby KAM tubes. In this particular case, at  $Re = 133$ , particles were poured into the stirred tank and swiftly distributed throughout the system except the KAM tubes. Particle focusing takes place almost immediately, and after a few minutes certain amount of particles have migrated into the vortices. As shown in **Figure 4**, two particle bands occupy 10–15% of the total fluid system, causing a highly inhomogeneous condition. This behaviour has been discussed in Ref. [8], and this trapping phenomenon was found for a number of different systems with different types of inertial particles.

We also conduct 3D particle trajectory velocimetry for a single finite-sized particle, and **Figure 5** shows the Lagrangian trajectory of a single one. We start the measurement at the moment when we introduce the particles into the system. The large dot is the particle position at  $t = 0$ . It is obvious that the particle follows a helical pattern through the impeller until it reaches the KAM tubes (as shown in **Figure 5a, c**). The particles move along the vortex tubes after they are ‘sucked’ into these specific regions (**Figure 5b**). We also calculate the residence time at the core of the vortex tube, and it is about 0.32 s [9].

Our theory is that when a particle is tiny, spherical and neutrally buoyant, it strictly follows the fluid streamline; by contrast, a large inertial particle can deviate the fluid flow essentially due to added inertia. The significance of size and density of the particle is captured by an inertia number

$$\sigma = \frac{St}{R} \text{ with } St = \frac{2}{9} \left( \frac{a}{L} \right)^2 Re, \quad R = \frac{1}{\frac{1}{2} + \frac{\rho_p}{\rho_L}} \quad (2)$$

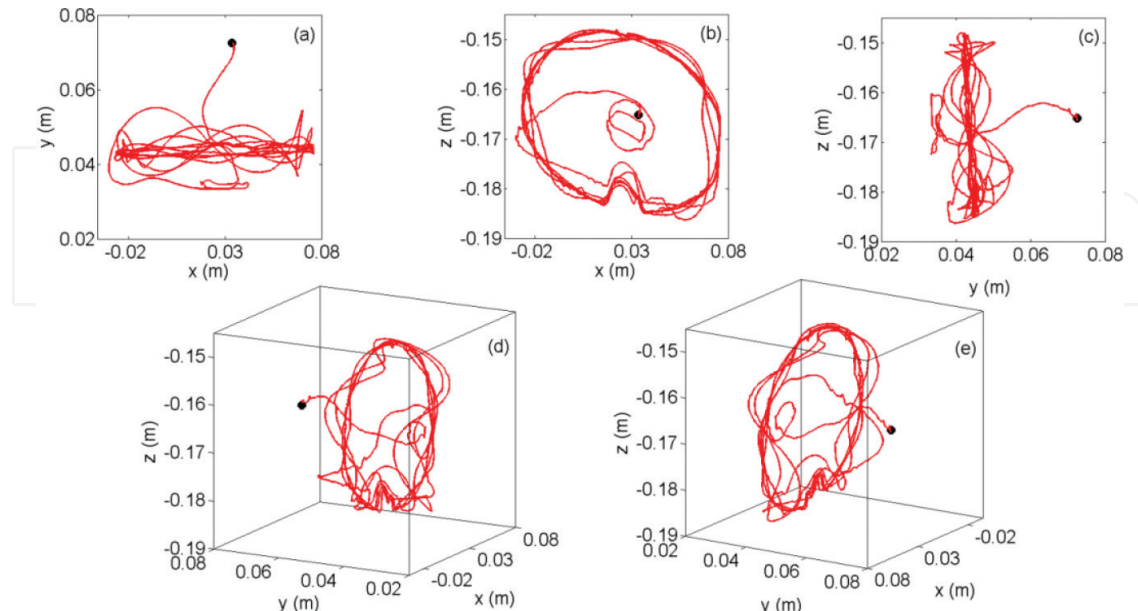


**Figure 5.** Tracking of Lagrangian positions of a single particle for a time interval of 7s from different views [9]. (a) x-y plane; (b) x-z plane; (c) y-z plane; (d)-(e) 3D trajectory

where  $a$  is the particle radius,  $L$  is the flow-length scale,  $St$  is the Stokes number,  $Re$  is the Reynolds number and  $R$  is the particle/fluid density ratio. The inertial factor  $\sigma$  is the ratio of the particle relaxation time and the typical time scale of the flow.  $\sigma$  is high, indicating that particle moves inertially and away from the underlying fluid streamline, while  $\sigma$  is smaller, suggesting that a particle moves passively. Sapsis and Haller derived a criterion for scattering regions (where particles do not follow their respective streamlines) in the flow in terms of the eigenvalue of a tensor. With further calculation, we have the scattering criteria:

$$\sigma\dot{\gamma} > 1 \quad (3)$$

where  $\dot{\gamma}$  is the local non-dimensional strain rate and  $\sigma\dot{\gamma}$  is interpreted as inertial stress. We note that the strain along streamline is proportional to the radius of curvature of the streamline. A particle can either follow a fluid streamline if it curves less, while scatters from the streamline when the streamline curves too much. As Eq. (3) is a local criterion, we further obtain a global instability criterion by using the strain- $Re$  relationship in the mixing tank. In laminar mixing tank, we have  $\dot{\gamma} = kRe$ , where  $k = 5$  for the impeller we use in the study. The global flow instability criterion is

$$k\sigma Re > 1 \quad (4)$$

We then substitute  $Re = \rho_f N L^2 / \mu$  into Eq. (4), and then we can calculate the minimum speed  $N_{\min}$  required to trigger the scattering and trapping phenomenon

$$N_{\min} = \frac{\mu}{aL\rho_f} \sqrt{\frac{9}{2} \frac{R}{k}} \times 60 \quad (5)$$

**Figure 6a** gives the minimum speeds required to trigger the focusing effect for particles with  $\rho_p/\rho_f = 0.5, 1$  and  $2$ , respectively, in the system. We can observe from **Figure 6a** that denser and smaller particles need higher speeds to trigger the instability.

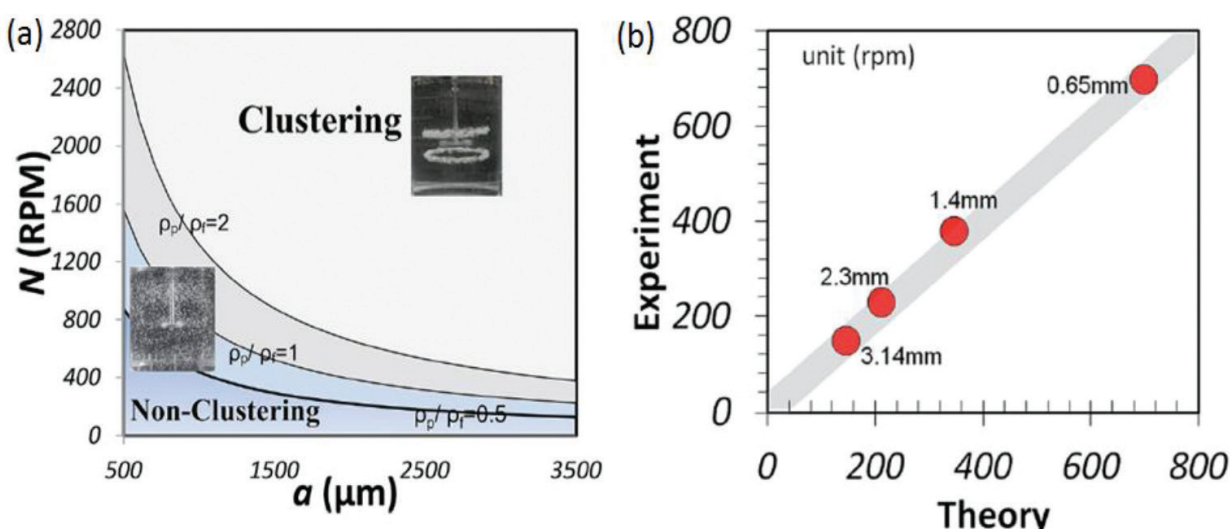


**Figure 6.** (a) Theory curves for critical speeds; (b) experiments versus theory.

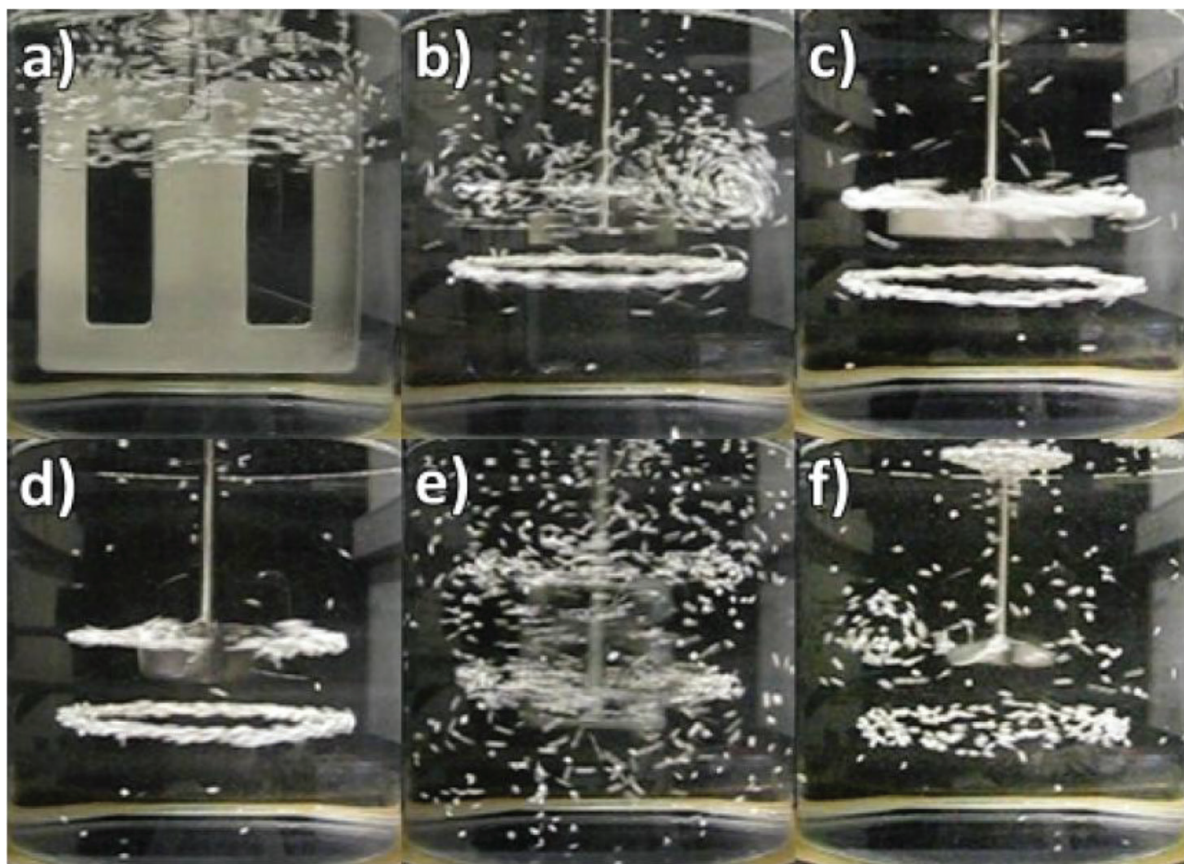


**Figure 7.** Photographs of the stirred vessel with particles after 15 min at highest speed for respective impeller. (a) Large impeller; (b) Rushton turbine; (c) Four-bladed impeller; (d) Two-bladed impeller; (e) Helical impeller; (f) Martin turbine.

The minimum clustering speed can be theoretically predicted from Eq. (5), and we compare the theory and experimental results in **Figure 6b**. It is remarkable that focusing of particles can occur when rotation speed reaches a predictable speed that relies on the particle and fluid properties. One more striking finding is that, we find that as long as the vortex tubes are present in the agitation system, clustering can take place in the mixing tank, irrespective of the impeller used for agitation. This is evident in **Figure 7**.

### 3. Particle classification phenomena in Taylor-Couette flow

Chemical and biochemical processes often have to separate, classify or disperse particles having various size and density. Wereley and Lueptow [10] numerically revealed that the motion of dilute, rigid and spherical particles with density greater than the fluid was determined by the interplay between the centrifugal force and the drag force in laminar Taylor vortex flow. They also found that particles approached a limit cycle orbit in  $r$ - $z$  cross-sectional plane and the limit cycle orbit of particle depended on the density and size of particle. Furthermore, even neutrally buoyant particles did not follow fluid streamlines exactly. Leighton and Acrivos [11] demonstrated in their experiments using a Couette device that neutrally buoyant particles might migrate across streamlines and against concentration gradients when undergoing bounded

shear flow. This chapter focuses on the particle classification phenomena in Taylor-Couette flow system that are discussed in the two cases of sedimenting and floating particles.

### 3.1. Experimental and numerical methods

Detailed information of experimental and numerical methods appears in our previous literature [12, 13]. **Figure 8** shows the experimental set-up with a measuring system. The concentric cylinder system consists of an inner cylinder of stainless steel and an outer cylinder of plexiglass in order to observe particle motions visually [12]. The outer diameter of the inner cylinder has 50 mm and the outer cylinder has 70 mm of the inner diameter. The length of cylinder system is 300 mm and the effective volume of the annular space is 550 cm<sup>3</sup>. The critical Reynolds number for the present radius ratio ( $\eta = 0.714$ ) can be estimated to be  $Re_c = 80.6$  by the linear stability theory [14]. The working fluid is an aqueous solution of glycerin having the density,  $\rho_f = 1050\text{--}1210 \text{ kg/m}^3$ . Each experimental observation was started after having passed enough time to form a stable vortex structure.

Fluorescent green dye was used as a passive tracer to visualize vortex structure. After adding the fluorescent green dye, the cross section of vortices was illuminated by a plane sheet of semiconductor laser light and the sequential visual data were taken by a digital video camera.

Polymethyl methacrylate (PMMA) particles suspended in the same aqueous solution of glycerol as the working fluid were fed into the top of the cylinder system at a very low flow rate whose axial Reynolds number ( $Re_{ax}$ ) was 0.42. The particle size was initially distributed from 10 to 80  $\mu\text{m}$ . Particle density,  $\rho_p$ , was distributed from 1200 to 1250  $\text{kg/m}^3$ . Hence, the density ratio,  $\beta = \rho_p/\rho_f$ , was 1.04–1.05, which means the density of the particle was slightly heavier than the fluid. The inlet concentration of particles was 0.26 wt% and the suspended solution was withdrawn using a hypodermic needle at regular intervals at 30 mm above the bottom of the apparatus. The sample solution was taken at both near the outer wall and in the vortex core.

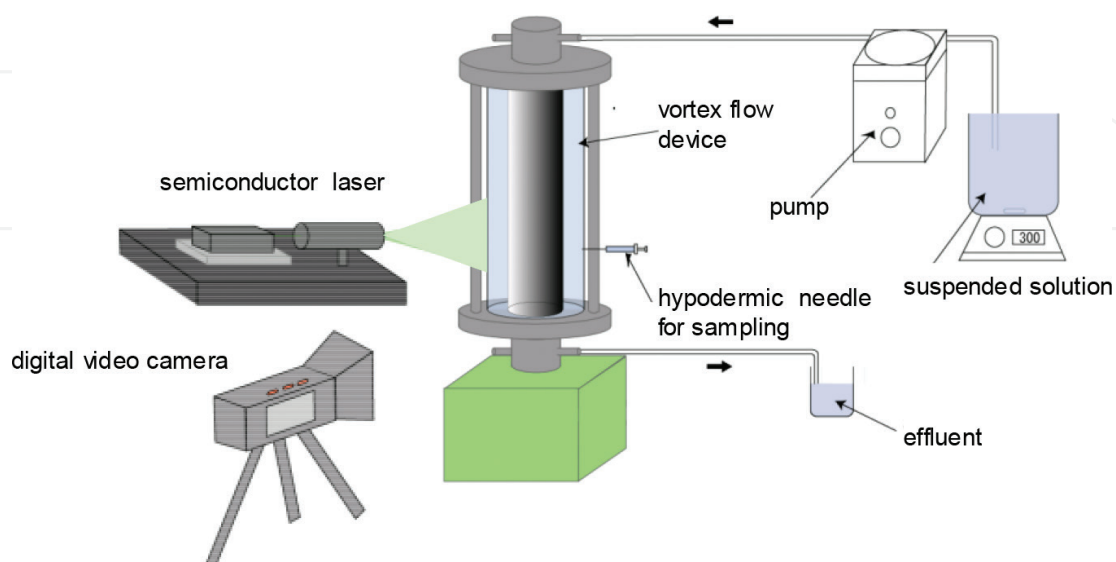


**Figure 8.** Experimental set-up [11].

The particle size distribution (PSD) of the sampled solution was obtained by measuring the size of particles with a microscope (KEYENCE, VHX-100N) on a number basis of percentage. About 200 particles were counted in the PSD measurements.

On the other hand, in the case of particle classification of floating particles, ion-exchanger acrylic resin particles (Amberlite, Organo Co.) were used [13]. The axial flow was not added in order to spatially fix axial classification patterns. They were sieved and classified into two groups with mean diameters of 710 and 974  $\mu\text{m}$ , respectively. Their densities  $\rho_p$  were measured to be  $1190 \text{ kg/m}^3$  from their buoyancy in an aqueous solution of glycerine (the density ratio,  $\rho_p/\rho_f = 0.98$ ). In order to distinguish between these two groups, the smaller and larger particles were dyed with red and blue, respectively. Two grams of each group of particles was initially added to the fluid from the top of the cylinder system. After that, the inner cylinder was rotated at a specific rotational speed [13]. After a steady-state fluid flow was established, the behaviour of the particles was observed using a digital video camera (NP-F960, Sony Co.) and the RGB intensity was measured at a certain time by using image-editing software (ImagePro Plus, Nippon Roper Co.) to characterize particle dispersion [13].

In the numerical simulation, a commercial computer fluid dynamics (CFD) code RFLOW (Rflow Co., Ltd.) was used for the simulation of the motion of particles. This numerical code is based on a finite-volume method and is enabled to simulate particle motion by a particle-tracking method and a (DEM) [13]. Numerical simulations were conducted under the same conditions as those used in the experiment, except the particle size and volumetric fraction of particles. Our works were conducted by using two different numerical simulation methods, namely a particle-tracking method and a DEM. For more detailed information about numerical simulation methods, refer to our previous works [12, 13].

### 3.2. Results and discussion

**Figure 9** shows cross-sectional views presenting axial diffusion process of tracer with measuring time from the injection of green dye. The Reynolds number and the axial Reynolds numbers were 200 and 0.42, respectively. As shown in **Figure 9**, the flow-visualization experiment using a laser-induced fluorescence method clearly revealed that there exist two distinct mixing regions in laminar Taylor vortex flow. The tracer near the vortex cell boundary was rapidly transported downward in the axial direction owing to the bypass flow effect. On the other hand, the fluid element was confined to the vortex core region without being exchanged with the outer flow region. In the case of PMMA particles whose density is slightly heavier than the working fluid, the centrifugal force or the shear-induced particle migration due to the rotation of inner cylinder displaces particles towards the wall of the outer cylinder and the larger particles tend to be located more on the outside in the vortex cell. Owing to the effect of the bypass flow, the larger particles in the outermost region of vortex cells more quickly disperse in the axial direction. Hence, we considered that particles can be classified by taking advantage of the bypass flow effect. **Figure 10** shows diagrams of PSD in the sampled solution and photographs of the particles corresponding to the PSDs [12]. Initially, the particle size distribution is relatively homogeneous in the range from 10 to 80  $\mu\text{m}$ . The population of particles smaller than 40  $\mu\text{m}$  is 52%, while that of particles larger than 40  $\mu\text{m}$  is 48%. Particles smaller than 50  $\mu\text{m}$  are dominant in the vortex core region at 42 min after feeding the suspended

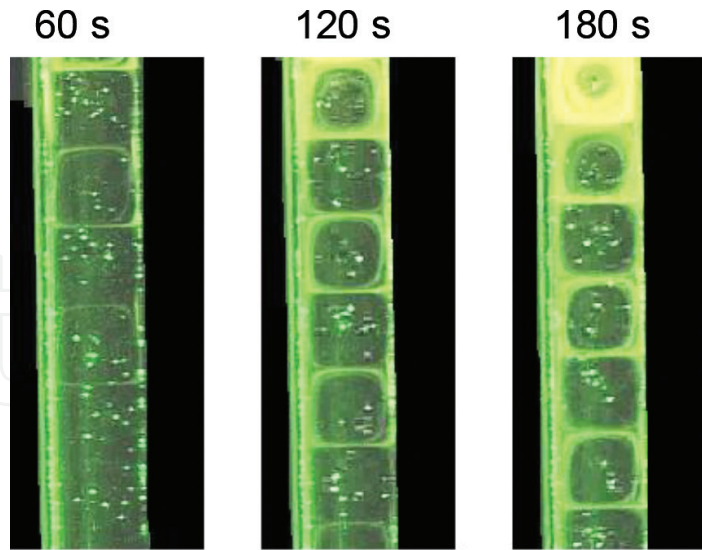


**Figure 9.** Cross-sectional views of axial diffusion of tracer green dye ( $Re = 200$  and  $Re_{ax} = 0.42$ ) [12].

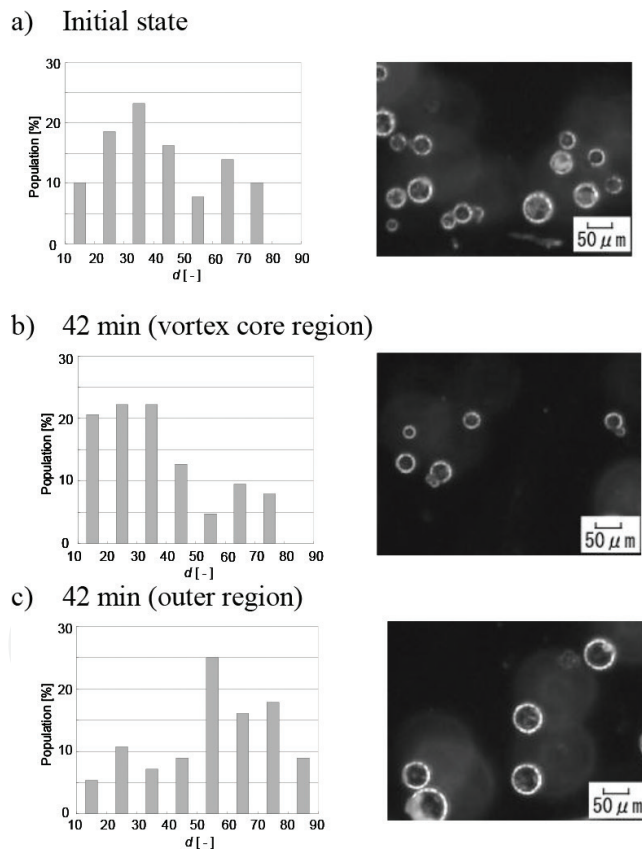


**Figure 10.** Particle size distribution and photographs [12]. a) Initial state; b) 42 min (vortex core); c) 42 min (outer region).

solution. The population of particles smaller than 50 μm is more than 75%. On the other hand, particles larger than 50 μm are dominant in the outer region of vortex and the population of particles larger than 50 μm almost reaches 70%. It can be, therefore, considered that the particles are classified by the size of 50 μm under this experimental condition. **Figure 11** shows

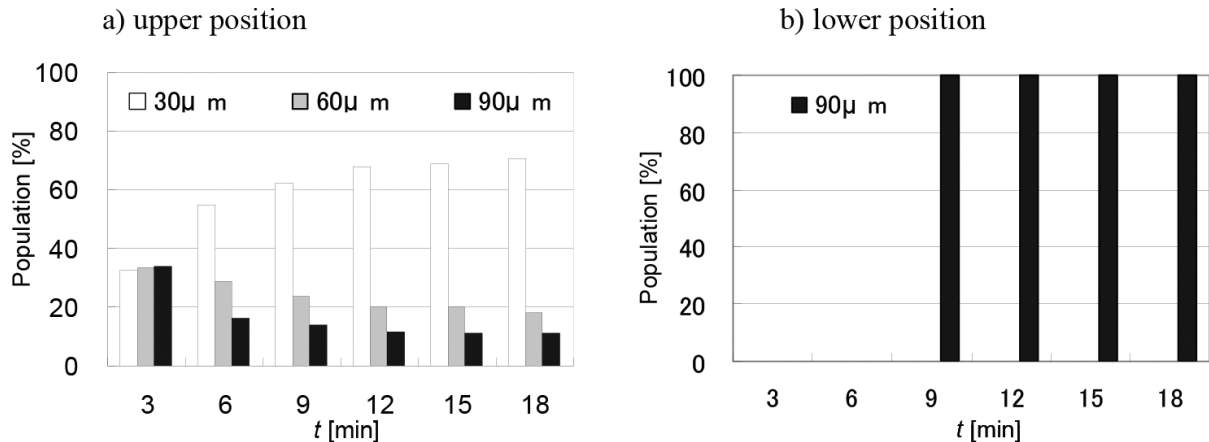


**Figure 11.** Time variation of PSD obtained by numerical simulation [12]. a) Upper position; b) Lower position.

the time variation of PSD numerically obtained in the upper portion (0–100 mm from the top) and the lower portion (200–300 mm from the top), respectively [12]. In the upper portion, the population of the smallest particles (30  $\mu\text{m}$ ) increases with time and reaches about 65% after 18 min. On the other hand, in the time variation of PSD obtained in the lower portion, only the largest particles can be seen even after 18 min. These numerical results suggest that particles can be classified and collected by installing several outlet ports in the axial direction even when the density difference is very small [12].

**Figures 12 and 13** show spatially fixed axial particle dispersion patterns and their corresponding RGB intensity variation in the axial direction in the case of floating particles [13]. **Figure 12** indicates that the particles penetrate deeper into the Taylor vortex flow region with increasing Reynolds number. In **Figure 12(a)**, the coloured region is classified into two layers and the first layer from the top dominantly contains blue particles (larger particles), and the second

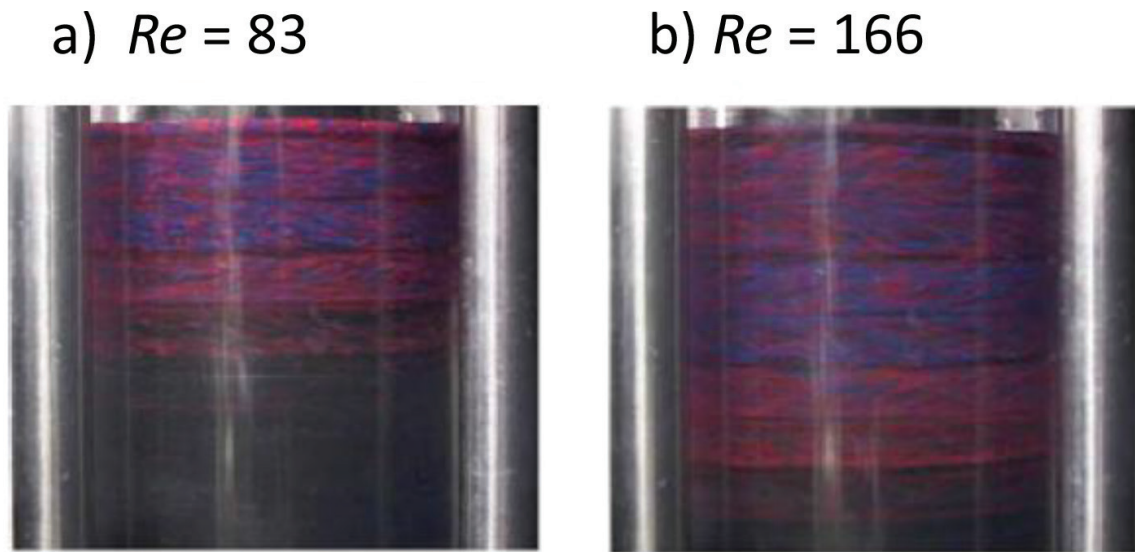


**Figure 12.** Front views of particle dispersion [13]. a)  $Re = 83$ ; b)  $Re = 166$ .

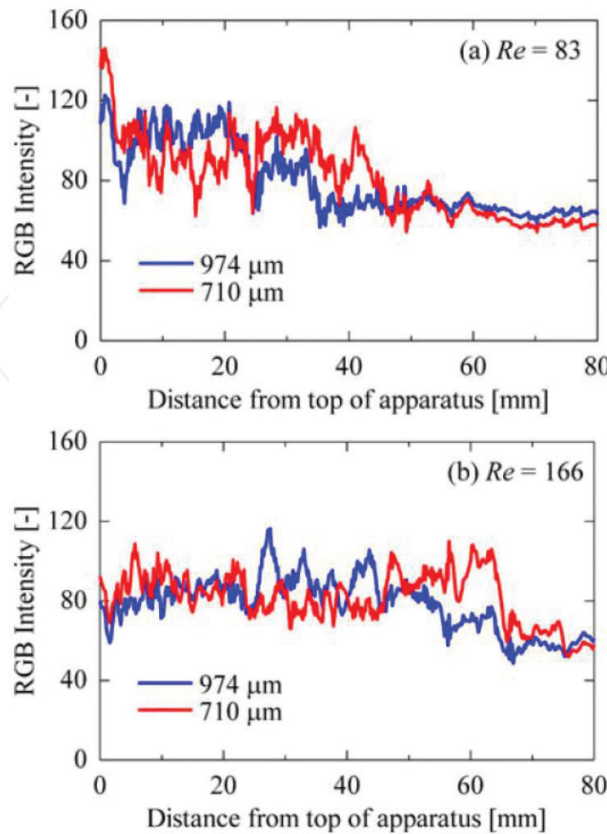


**Figure 13.** RGB intensity against axial distance from the top of apparatus [13]. (a)  $Re = 83$ ; (b)  $Re = 166$ .

layer dominantly contains red ones (smaller particles). On the other hand, in **Figure 12(b)**, the coloured region is classified into three layers. The first layer seems to have blue and red particles evenly. The second layer contains more blue particles and the third layer contains more red ones.

These images show that the red and blue particles were segregated. To clarify this behaviour, the results of a qualitative evaluation by variation of RGB intensity are shown in **Figure 13** [13]. For  $Re = 83$ , the high-intensity region for blue lies between 10 and 30 mm, while that for red lies between 30 and 50 mm.  $Re$  increases to 166, the high-intensity region for blue shifts downward to about 30–50 mm, while that for red shifts to about 50–70 mm [13]. However, the width of the high-intensity region for each colour remains constant at about 20 mm, irrespective of the rotational speed [13]. As the gap between the inner and outer cylinders is 10 mm, the vertical vortex cell length, which corresponds to half of the axial wavelength, is about 10 mm. Hence, 20 mm of the axial length corresponds to the length of a pair of two counter-rotating vortices. Flow visualization also supported that these regions correspond to pairs of two counter-rotating vortices surrounded by inflow cell boundaries. These results indicate that particles of the same size tend to aggregate within a certain pair of vortices and smaller particles can penetrate deeper into the Taylor vortex flow region than larger particles.

**Figure 14** shows the  $r$ - $z$  cross-sectional plane of particle orbits which was numerically obtained for each size [13]. Contrary to the previous case of sedimenting particles, the smaller

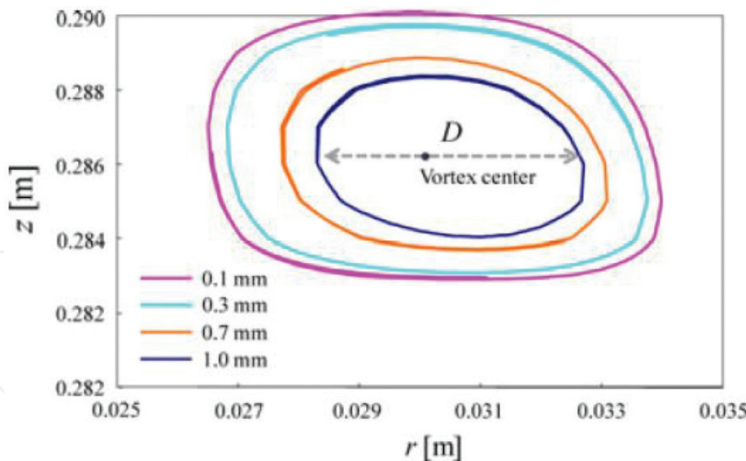


**Figure 14.**  $r$ - $z$  cross sections of particle orbits in the particle-tracking method at  $Re = 207.5$  for four particles of different sizes [13].

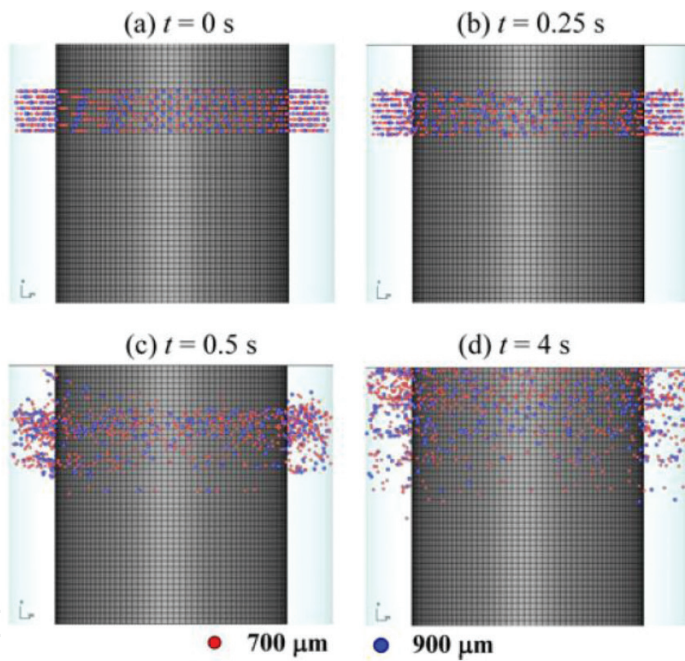


**Figure 15.** Particle diffusion process obtained by the DEM ( $Re = 166$ ) (axial distance range: 0.24–0.30 m) [13]. (a)  $t = 0$  s; (b)  $t = 0.25$  s; (c)  $t = 0.5$  s; (d)  $t = 4$  s

particles move along the outer orbit on a torus. This result indicates that small particles may be exchanged between vortices owing to a bypass flow that exists in the outer region of each vortex as previously mentioned. However, the effect of bypass flow in the case without axial flow is smaller than in the case with axial flow. The DEM revealed two possible mechanisms for axial transport of particles in the axial direction. One is that the axial particle dispersion can result from the unsteadiness due to vortex development from the rest as shown in **Figure 15** [13]. The other is that particle collision can induce axial particle transportation. **Figures 16** and **17** show drag force acting on a particle and correlation between interparticle collision

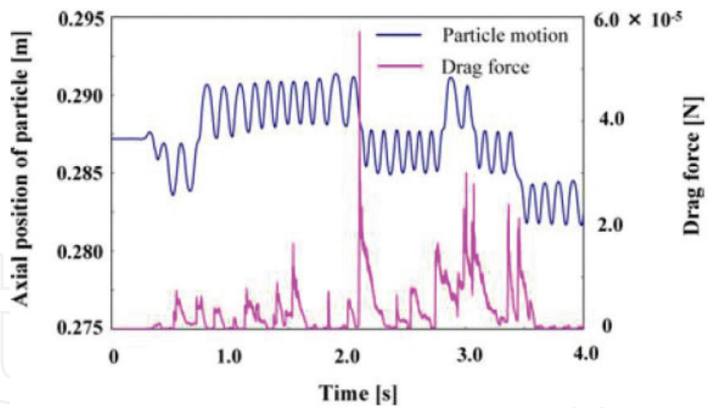


**Figure 16.** Effect of drag force acting on a particle at different axial position [13].

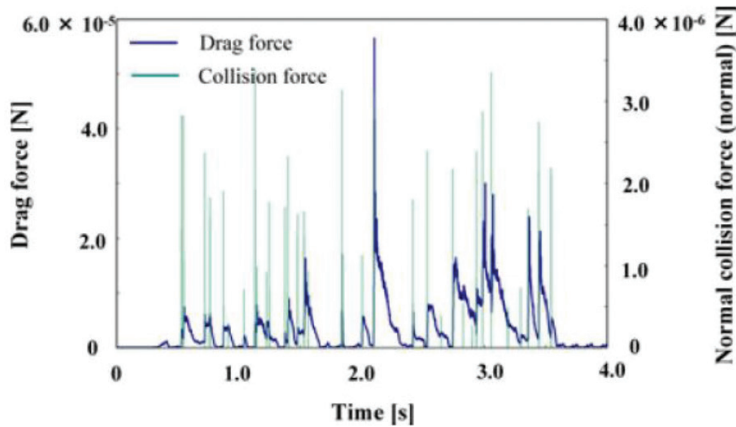


**Figure 17.** Correlation between interparticle collision and drag force [13].

and drag force [13]. In these figures, a particle is arbitrarily chosen by the DEM simulation. **Figure 16** shows the relation between the axial position of a 700- $\mu\text{m}$  particle and the drag force acting on the particle. It has been found that a large drag force is generated during the motion of the particle over a vortex cell boundary, especially during motion towards a lower vortex. The relation between the drag force acting on the particle and interparticle collision is shown in **Figure 17**. The peaks corresponding to normal collision force indicate that the particle collides with another particle. As seen in **Figure 17**, the drag force acts on the particle just after collision in almost all the cases. Therefore, particle transfer across a vortex cell boundary is inferred to occur at the moment of a particle collision.

#### 4. Conclusions

This chapter introduced particle clustering in stirred vessels and particle classification in Taylor vortex flow based on our previous research works [8, 12, 13]. For particle clustering phenomena, to the authors' best knowledge, no universal agreement has been made on the tendency of inertial particle motion in laminar flow system. In this study, we found that inertial

particles can move away from their streamlines in the chaotic flow regions and subsequently migrate into the vortex tubes. The chaos-vortex flow structure can be easily triggered in many stirred systems; we thus expect that this trapping phenomenon can be encountered in a number of systems. For particle classification in Taylor vortex flow, on the other hand, particles having various sizes can be classified by taking account of the vortex motion and the bypass flow near the outer edge of vortices. In this case, the centrifugal force and the shear-induced migration due to the rotation of inner cylinder play the important role for moving larger particles more outside in the vortex cell.

From the viewpoints of process intensification, the following applications may be considered. Firstly, clustering particles can easily eliminate isolated mixing regions, which are an obstacle for global mixing in a stirred vessel [15, 16]. The advantage of this method is simpler and less reliant on energy input, because shorter mixing time can be obtained at very low Reynolds number even without inserting baffles. Secondly, Wang et al. [8] proposed a novel solid-liquid separation technique using a conventional mixing vessel, as shown in **Figure 18**. The conceptual design can find utility in a number of applications including the production of celluloid, fat and oils, cellulose ethers, gelatin and starch. To achieve more effective separations, stirred separators should be connected either in series or in parallel to maximize the throughput [8].

As for particle classification phenomena, an integrated process with granulation and classification can be considered. In fact, Kim et al. [17] proposed a novel crystallizer which simultaneously classifies the crystals utilizing vortex moving. Larger particles are moving

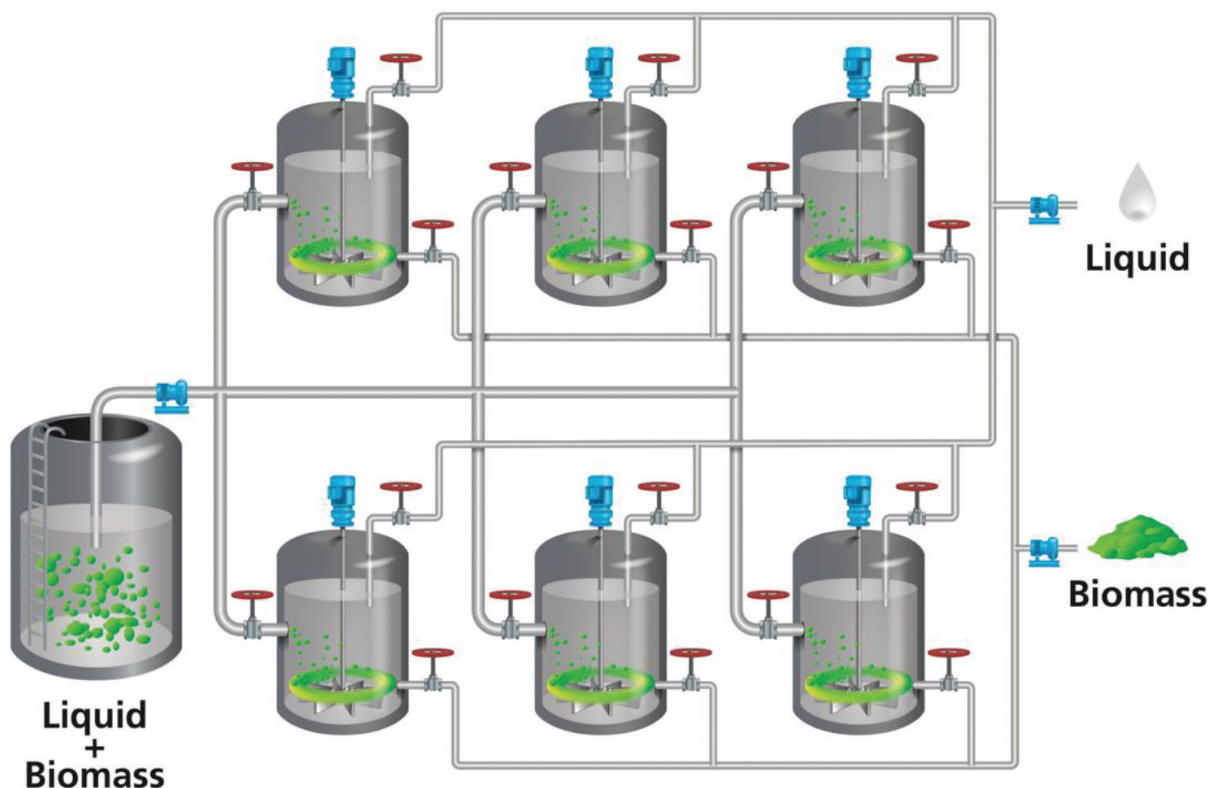


**Figure 18.** A conceptual design for biomass-liquid separation applied in biorefinery [8].

downward and smaller particles are moving upward. Small and large particles are obtained separately from the top outlet and bottom outlet, respectively. The flow characteristics of Taylor vortex flow are quite similar to the Dean vortex flow. Ookawara et al. [18] proposed a micro-separator/classifier having a curved microchannel with a rectangular cross section. This micro-separator/classifier takes advantages of the effects of centrifugal force and Dean vortices generated at the curve channel. This clearly indicates that the particle classification phenomena can be applied to micro-flow processes.

## Author details

Steven Wang<sup>1</sup> and Naoto Ohmura<sup>2\*</sup>

\*Address all correspondence to: ohmura@kobe-u.ac.jp

1 Department of Chemical Engineering and Advanced Materials, Newcastle University, Newcastle upon Tyne, United Kingdom

2 Department of Chemical Science and Engineering, Kobe University, Kobe, Japan

## References

- [1] Mackely M. R., Ni. X. Mixing and dispersion in a baffled tube for steady laminar and pulsatile flow. *Chemical Engineering Science*. 1991;46(12):3139–3151. DOI: 10.1016/0009-2509(91)85017-R
- [2] Reay D., Ramshaw C., Harvey A. *Process Intensification*. 1st ed. Oxford, UK: Butterworth-Heinemann; 2008. 444 p.
- [3] Harvey A. P., Stonestreet P. A mixing-based design methodology for continuous oscillatory baffled reactors. *Chemical Engineering Research and Design*. 2002;80(1):31–44. DOI: 10.1205/026387602753393204
- [4] Kataoka K., Doi H., Hongo T., Futagawa M. Ideal plug-flow properties of Taylor vortex flow. *Journal of Chemical Engineering of Japan*. 1975;8(6):472–476. DOI: 10.1252/jcej.8.472
- [5] Jung W. M., Kang S. H., Kim W-S., Choi C. K. Particle morphology of calcium carbonate precipitated by gas–liquid reaction in a Couette–Taylor reactor. *Chemical Engineering Science*. 2000;55(4):733–747. DOI: 10.1016/S0009-2509(99)00395-4
- [6] Kataoka K., Ohmura N., Kouzu M., Simamura Y., Okubo M. Emulsion polymerization of styrene in a continuous Taylor vortex flow reactor. *Chemical Engineering Science*. 1995;50(9):1409–1416. DOI: 10.1016/0009-2509(94)00515-S
- [7] Giordano R. L. C., Giordano R. C., Cooney C. L.. Performance of a continuous Taylor–Couette–Poiseuille vortex flow enzymic reactor with suspended particles. *Process Biochemistry*. 2000;35(10):1093–1101. DOI: 10.1016/S0032-9592(00)00143-6

- [8] Wang S., Metcalfe G., Stewart R. L., Wu J., Ohmura N. Feng X. et al.. Solid-liquid separation by particle-flow-instability. *Energy & Environmental Science*. 2014;7(12):3982–3988. DOI: 10.1039/C4EE02841D
- [9] Gulan U., Holzner M., Jiang M., Windhab E., Wang S. Visualization of particle focusing in chaotic flow. *Journal of Visualized Experiments*, in press, 2016
- [10] Wereley S. T., Lueptow R. M. Velocity field for Taylor–Couette flow with an axial flow. *Physics of Fluids*. 1999;11(12):3637–3649. DOI: 10.1063/1.870228
- [11] Leighton D., Acrivos A. The shear-induced migration of particles in concentrated suspensions. *Journal of Fluid Mechanics*. 1987;181:415–439. DOI: 10.1017/S0022112087002155
- [12] Ohmura N., Suemasu T., Asamura Y. Particle classification in Taylor vortex flow with an axial flow. *Journal of Physics: Conference Series*. 2005;14:64–71. DOI: 10.1088/1742-6596/14/1/009, Suemasu
- [13] Saomoto K., Horie T., Kumagai N., Takigawa T., Noui-Mehidi M. N., Ohmura N.. Dispersion of floating particles in a Taylor vortex flow reactor. *Journal of Chemical Engineering of Japan*. 2010;43(4):319–325. DOI: 10.1252/jcej.09We07
- [14] Di Prima R. C., Swinney H. L. Instabilities and transition in flow between concentric rotating cylinders. In: Swinney H. L., Gollub J. P., editors. *Hydrodynamic Instabilities and the Transition to Turbulence*. 1st ed. Berlin Heidelberg, Germany: Springer-Verlag; 1981. pp. 139–180.
- [15] Alatengtuya, Nishioka N., Horie T., Noui-Mehidi M. N., Ohmura N. Effect of particle motion in isolated mixing regions on mixing in stirred vessel. *Journal of Chemical Engineering of Japan*. 2009;42(10):459–463. DOI: 10.1252/jcej.09we087
- [16] Takahashi K., Motoba M. Chaotic mixing created by object inserted in a vessel agitated by an impeller. *Chemical Engineering research and Design*. 2009;87(4):386–390. DOI: 10.1016/j.cherd.2009.01.003
- [17] Kim S. J., Kim D. H., Gu b., Kim, D. Y., Yang D. R.. Simulation of Taylor–Couette reactor for particle classification using CFD. *Journal of Crystal Growth*. 2013;373:106–110. DOI: 10.1016/j.jcrysgro.2012.12.006
- [18] Ookawara S., Higashi R., Dstreet D., Ogawa K. Feasibility study on concentration of slurry and classification of contained particles by microchannel. *Chemical Engineering Journal*. 2004;101(1–3):171–178. DOI: 10.1016/j.cej.2003.11.008